Magnetization profile and core-level spectroscopy in a multiply quantized vortex of imbalanced Fermi superfluids

K. M. Suzuki,[*] T. Mizushima,[†] M. Ichioka, and K. Machida

Department of Physics, Okayama University, Okayama 700-8530, Japan

(Received 25 February 2008; published 18 June 2008)

The core structure of multiply quantized vortices is theoretically investigated in a fermionic superfluid near Feshbach resonance. Under population imbalance in two hyperfine spin states, the vortex core is filled in by the "paramagnetic moment." Here, we find the spatial oscillation of the magnetization inside the core sensitively due to the topological structure of the pairing field, in the range from the weak-coupling regime to the unitary limit. This magnetization inside the giant core reveals the winding number of the vortex and directly results from the low-lying quasiparticle states bound inside the core. It is therefore proposed that the density profile experiment using phase contrast imaging can provide the spectroscopy of novel core level structures in giant vortices. To help understand these outcomes, we also derive an analytic solution for the low-lying quasiparticle states inside the core of a multiply quantized vortex.

I. INTRODUCTION

Much attention has been focused on quantized vortices of both bosonic and fermionic superfluids. In the bosonic system, the order parameter is directly associated with the particle density, which is observable via the absorption image in experiments. Hence, the vortex core, defined as the zeros of the order parameter, can be visualized via the absorption image in the Bose-Einstein condensate (BEC) of ultracold atoms, which has provided an opportunity to investigate both the static and dynamic properties of vortices [1,2].

In the fermionic case, however, the situation is drastically changed, where the order parameter corresponds to the wave function of the Cooper pair and thus the visualization of vortices is not trivial. The particle density is sensitively affected by the quasiparticle structure with an eigenenergy close to the Fermi energy E_F. A pioneering work in 1964 [3] revealed the fact that for a singly quantized vortex state in the s-wave case, a novel quasiparticle state exists tightly bound in the core region $\sim \xi$ called the Caroli–de Gennes–Matricon (CdGM) state. The important points to note are as follows. (i) The eigenenergy of the CdGM state of the vortex core is embedded in the low-energy region $E/E_F = 2/(k_F \xi)^2$ with k_F being the Fermi wave number [3], and its lowest energy level is slightly shifted from the Fermi level. Also, (ii) the eigenenergy inside the core is well discretized. Hence, the spectrum of the quasiparticle states yields the particle-hole asymmetry inside the core [4]. It has been found that due to the asymmetric and discretized spectrum of the CdGM state, the particle density can be suppressed inside the core [5], called the "quantum depletion," which makes a vortex visible via the density profile even in the Fermi system. The depletion can be gradually enhanced as the core radius ξ approaches the mean interparticle distance k_F^{-1}, i.e., the quantum limit [5–12]. This fact is directly observed in ultracold atomic systems under Feshbach resonance [13].

The microscopic studies on multiply quantized or giant vortices have been carried out in the type-II superconductors [14–18], which indicate that the number of the branch of the CdGM state is closely associated with the topological structure of the order parameter [14]. Recently, a macroscopic manifestation of giant vortices in neutral fermionic atoms was theoretically studied by Hu and Liu [19], who found the oscillating pattern of the particle density profiles inside the core in the population balanced system.

The giant vortex state in ultracold Fermi atoms has not been experimentally accomplished so far. In BEC's, in contrast, the giant vortices have been experimentally created by using several techniques: The topological phase imprinting method [20–22], a fast rotating BEC confined in a quadratic plus quartic trap [23], and the transfer of the orbital angular momentum from Laguerre-Gaussian photons to a BEC [24]. In addition, the Feshbach resonance, which controls the s-wave scattering length a, enables one to continuously connect the BEC with the fermionic superfluid, i.e., the BEC to Bardeen-Cooper-Schrieffer (BCS) crossover. By sweeping the magnetic field, the BEC of long-lived molecules in $a > 0$ can be transferred into the Cooper pair of fermionic atoms with the weak attractive interaction $a < 0$, across the unitary limit $a \to \pm \infty$.

In this paper, we propose a manifestation due to the topological structure of the order parameter with a multiply quantized vortex. Under population imbalance in two hyperfine spin states ($\uparrow$ and $\downarrow$ spins), the occupation difference of the CdGM state makes the core of a singly quantized vortex with the winding number $w = 1$ be magnetized [25,26]. Here, in the BCS regime $a < 0$, by solving the Bogoliubov–de Gennes (BdG) equation under population imbalance, we find that the magnetization profile inside the core of the multiply quantized vortex yields an oscillation pattern with several peaks located on a concentric circle. This oscillation is well understandable from the novel quasiparticle embedded in the vicinity of E_F. To help this understanding, we also derive the analytic solution for the CdGM states in multiply quantized vortices, by following the procedure which was proposed by Caroli *et al.* [3]. The analysis is extended to the vicinity of

---

*kenta@mp.okayama-u.ac.jp

†mizushima@mp.okayama-u.ac.jp

the unitary limit $(a \to \infty)$ of harmonically trapped Fermi gases. Here, we discuss that in the BCS-BEC crossover, the oscillation pattern in the magnetization profile inside the core is changed from that in the BCS regime due to the strong-coupling effect, which embodies the shift of the energy level of the low-lying CdGM state.

This paper is organized as follows. In Sec. II, after introducing the theoretical framework based on the BdG equation, we present the numerical results on multiply quantized vortex states under population imbalance. This is carried out in the weak-coupling regime in Sec. II. The analysis is extended to trapped Fermi gases with population imbalance in the vicinity of Feshbach resonance in Sec. III. Here, we discuss the crossover from the weak-coupling regime to the Feshbach resonance region. Following the previous work [27], we introduce the regularization of the gap equation and the particle number equation, which allows one to describe the microscopic structure in the BCS-BEC crossover. Then, we shall show the numerical results on the macroscopic and quasiparticle structures in resonant Fermi systems with giant vortices. The final section is devoted to conclusions and discussions. In the Appendix, the details on the analytical solution of the BdG equation in giant vortices shall be described. Throughout this paper, we put $\hbar = k_B = 1$.

II. GIANT VORTICES WITH POPULATION IMBALANCE: WEAK COUPLING LIMIT

A. Theoretical framework

Let us consider a single vortex state with arbitrary winding number $w \geq 1$, where the pair potential can be expressed in the cylindrical coordinate $\mathbf{r} = (r, \theta, z)$ as

$$\Delta(\mathbf{r}) = \Delta(r)e^{iw\theta}. \quad (1)$$

Without the loss of generality, $\Delta(r)$ is a real function. We start with the BdG equation for the quasiparticle wave function $u_q(\mathbf{r})$ and $v_q(\mathbf{r})$ labeled by the quantum number $\mathbf{q}$ [26–30]

$$\begin{bmatrix} \mathcal{K}_\uparrow(\mathbf{r}) & \Delta(\mathbf{r}) \\ \Delta^*(\mathbf{r}) & -\mathcal{K}_\downarrow(\mathbf{r}) \end{bmatrix} \begin{bmatrix} u_q(\mathbf{r}) \\ v_q(\mathbf{r}) \end{bmatrix} = E_q \begin{bmatrix} u_q(\mathbf{r}) \\ v_q(\mathbf{r}) \end{bmatrix}. \quad (2)$$

The single particle Hamiltonian is given by $\mathcal{K}_\sigma(\mathbf{r}) = -\frac{\nabla^2}{2M} - \mu_\sigma + V(\mathbf{r})$, where M is the mass of fermions and $\mu_{\uparrow,\downarrow} = \mu \pm \delta\mu$ is the chemical potential of the spin σ state. $V(\mathbf{r})$ denotes a background potential. Here, we impose the periodic boundary condition along the z axis with the period L. Since the resulting system yields the axisymmetry, the quasiparticle wave function may be expressed by

$$\begin{bmatrix} u_q(\mathbf{r}) \\ v_q(\mathbf{r}) \end{bmatrix} = e^{iq_z z} \begin{bmatrix} u_q(r)e^{iq_\theta \theta} \\ v_q(r)e^{i(q_\theta - w)\theta} \end{bmatrix}, \quad (3)$$

where the eigenstate is labeled by the quantum number $\mathbf{q} = (q_r, q_\theta, q_z)$ with $q_\theta = 0, \pm 1, \pm 2, \ldots$ and $q_z = 0, 2\pi/L, 4\pi/L, \ldots$.

The BdG Eq. (2) is self-consistently coupled with the gap equation given by

$$\Delta(\mathbf{r}) = g \sum_{|E_q| < E_c} u_q(\mathbf{r}) v_q^*(\mathbf{r}) f(E_q), \quad (4)$$

where $f(E_q) = 1/(e^{E_q/T} + 1)$ is the Fermi distribution function, E_c is the energy cutoff, and g is the coupling constant. Because of the breaking of the particle-hole symmetry due to the chemical potential shift $\delta\mu/2 \equiv \mu_\uparrow - \mu_\downarrow$, the sum in Eq. (4) is carried out for all eigenstates with both the positive and negative eigenenergies. Throughout this paper, we set $\delta\mu \geq 0$, which means the spin-up component becomes the majority.

In this section, in order to focus on the vortex core, we restrict our attention to the vortex state with the weak pair potential $\Delta_0 = 0.1E_F$ in the absence of a background potential, i.e., $V(\mathbf{r}) = 0$. Here Δ_0 is the pair potential in the bulk at $T = 0$, and E_F is the Fermi energy in an ideal Fermi gas. Then, the BdG Eq. (2) can be numerically solved by using the Bessel function expansion [31]

$$\begin{bmatrix} u_q(r) \\ v_q(r) \end{bmatrix} = e^{iq_z z} e^{iq_\theta \theta} \sum_{i=1}^{N_B} \begin{bmatrix} C_i^{(q_\theta q_z)} \varphi_i^{(q_\theta)}(r) \\ e^{-iw\theta} D_i^{(q_\theta q_z)} \varphi_i^{(q_\theta - w)}(r) \end{bmatrix}, \quad (5)$$

where the basis function

$$\varphi_i^{(\nu)}(r) \equiv \frac{\sqrt{2}}{R J_{\nu+1}(\alpha_i^{(\nu)})} J_\nu\left(\frac{\alpha_i^{(\nu)}}{R} r\right) \quad (6)$$

satisfies the orthonormal condition $\int_0^R \varphi_i^{(\nu)}(r) \varphi_j^{(\nu)}(r) r dr = \delta_{i,j}$. Here J_ν is the νth Bessel function and $\alpha_i^{(\nu)}$ is the ith zero of J_ν. Throughout this section, all physical quantities are scaled by the length unit $k_F^{-1} \equiv \sqrt{2ME_F}$ and the energy unit E_F, and we fix the radius of the cylinder $R = 200k_F^{-1}$, the height $L = 50k_F^{-1}$, the number of the basis function $N_B = 100$, and the chemical potential $\mu = E_F$. Note that the situation described in this section is applicable not only to ultracold Fermi atoms but also to superconductors under a magnetic field, acting on electron spins.

B. Quasiparticle structure and local magnetization inside giant cores

In an isolated vortex with arbitrary winding number $w \geq 1$, the eigenenergy of the CdGM state, whose wave function is localized around the core, is analytically given from the BdG Eq. (2) as

$$E_q = -\left(q_\theta - \frac{w}{2}\right)\frac{\omega_0}{\sin(\alpha)} + \left(n + \frac{w-1}{2}\right)\sin(\alpha)\omega_1, \quad (7)$$

with $n = 0, \pm 1, \pm 2, \ldots$, and $q_\theta = 0, \pm 1, \ldots$. We also introduce $\sin^2(\alpha) \equiv 1 - q_z^2/(2M\mu)$. For simplicity, from now on, we consider the eigenstates with $q_z = 0$, i.e., $\alpha = \pi/2$. The two coefficients $\omega_{0,1}$ are shown in Eq. (A19) and the details on the derivation of Eq. (7) are also described in the Appendix.

The expression of E_q in Eq. (7) is composed by two different energy scales: (i) The energy scale comparable with the pair potential $\omega_1 \sim \Delta_0$ and (ii) the much smaller energy scale $\omega_0 \sim \Delta_0^2/E_F \ll \omega_1$ in the weak-coupling limit $\Delta_0 \ll E_F$. For a single vortex state with $w = 1$, the lowest branch of the dispersion relation, i.e., $n = 0$, reproduces the well-known CdGM eigenstate with $E_q \simeq -\frac{\Delta_0^2}{2E_F}(q_\theta - \frac{1}{2})$ [3]. The lowest
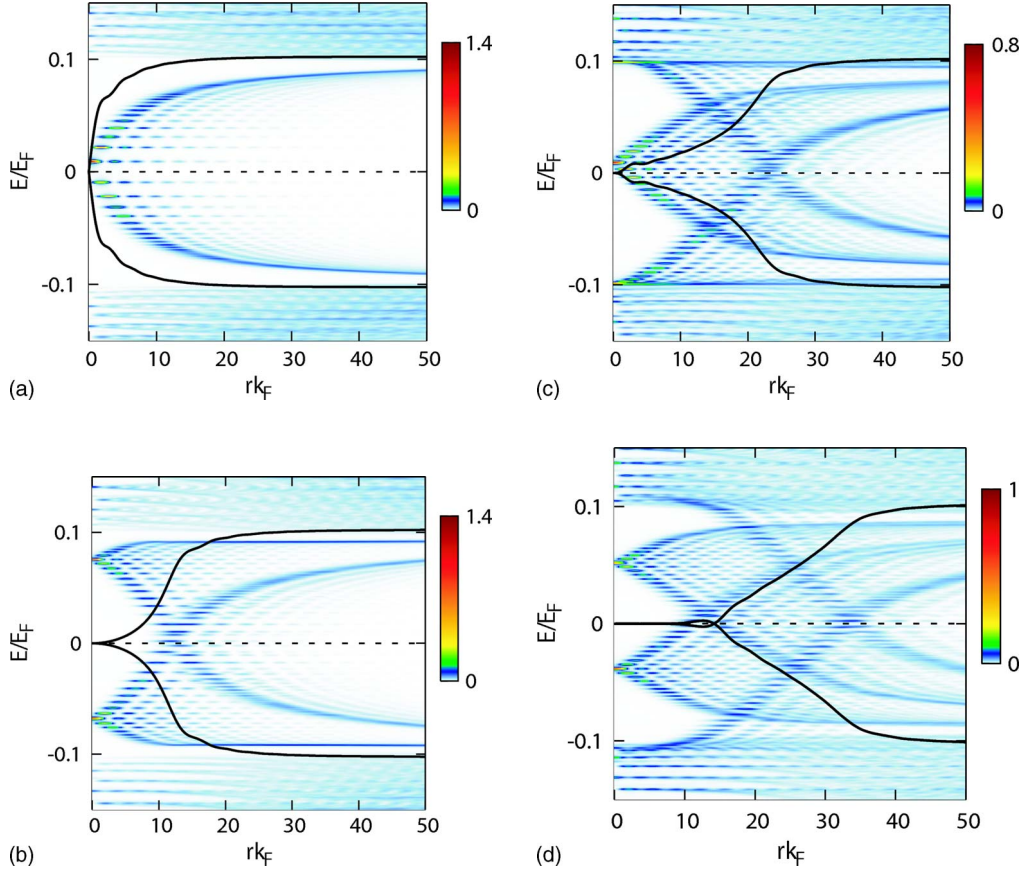
FIG. 1. (Color online) Local density of states $\mathcal{N}(r,E)$ around the core in multiply quantized vortices without population imbalance in the case of $w=1$ (a), $w=2$ (b), $w=3$ (c), and $w=4$ (d) at $T=0$, where only the eigenstates with $q_z=0$ are taken into account. The solid line shows the corresponding local pair potential $\pm\Delta(r)$. Throughout this paper, the Fermi surface at $\delta\mu=0$ is put on $E=0$.

CdGM state yields the "pseudozero" energy $E_q \sim \Delta_0^2/E_F$ $\ll \Delta_0$ in the weak-coupling regime. The wave function is localized in the core region within $r \lesssim \xi$ [see Fig. 1(a)], where ξ is the coherence length, $\xi \equiv k_F/(M\Delta_0)$, and characterizes the core radius of the $w=1$ vortex. In addition, Eq. (7) for arbitrary winding number $w \geq 1$ is in good agreement with the result obtained from the semiclassical approximation [18].

Here, two important facts arising from Eq. (7) should be mentioned. (i) For an odd number of vorticity w, a core bound CdGM state always exists with the pseudozero energy and $q_\theta=0$, because the second term in Eq. (7) can vanish. In general, the wave function is well expressed by Eq. (A3) in the region within $r \ll \xi$, i.e., $u_q(r) \sim J_{q_\theta}(k_F r) \sim (k_F r)^{|q_\theta|}$. Hence, the wave function of the lowest CdGM state with $q_\theta=0$ may have a large intensity on the vortex center. In contrast, the pseudozero "core bound" state with $q_\theta=0$ never appears in the case of the even number w, because the second term in Eq. (7) remains finite. The energy of the low-lying state on the vortex center is of the order of Δ_0. (ii) Apart from the core bound state with $q_\theta=0$, for $w>1$, there may exist a state with pseudozero energy $E_q \sim 0$ even in the even number of w when $|q_\theta| \sim O(k_F\xi)$. In addition, the number of such a state is determined by the winding number of vortices, as we will show below. Hence, it is concluded that the pseudozero energy states can appear inside or around a

giant vortex core with arbitrary winding number, while the peak position of the wave function sensitively depends on the winding number, namely, the topological structure of $\Delta(r)$.

To numerically confirm the direct relation between the winding number and the pseudozero energy states, it is worthwhile to visualize the quasiparticle structure of the w-fold quantized vortex in balanced systems. Here, we introduce the local density of states (LDOS) $\mathcal{N}_\sigma(r,E)$, which is given by

$$\mathcal{N}_\uparrow(r,E) = \sum_q |u_q(r)|^2 \delta(E - E_q), \quad (8a)$$

$$\mathcal{N}_\downarrow(r,E) = \sum_q |v_q(r)|^2 \delta(E + E_q). \quad (8b)$$

Figure 1 shows the LDOS for vortex states with $w=1,2,3,4$ in the case of population balance $\delta\mu=0$, where $\mathcal{N}(r,E) \equiv [\mathcal{N}_\uparrow(r,E)+\mathcal{N}_\downarrow(r,E)]/2$. In the core of the odd-number vortex ($w=1,3$), the lowest eigenstate is situated at $r=0$ and in the vicinity of the Fermi level ($E \sim 0$). As we have mentioned above, the vortex state with the even w has the distinct energy gap on the center of the vortex, where the excitation spectrum is almost symmetric with respect to the Fermi level. The CdGM branches in the giant vortex with $w>1$ always touch the zero energy in the position far from

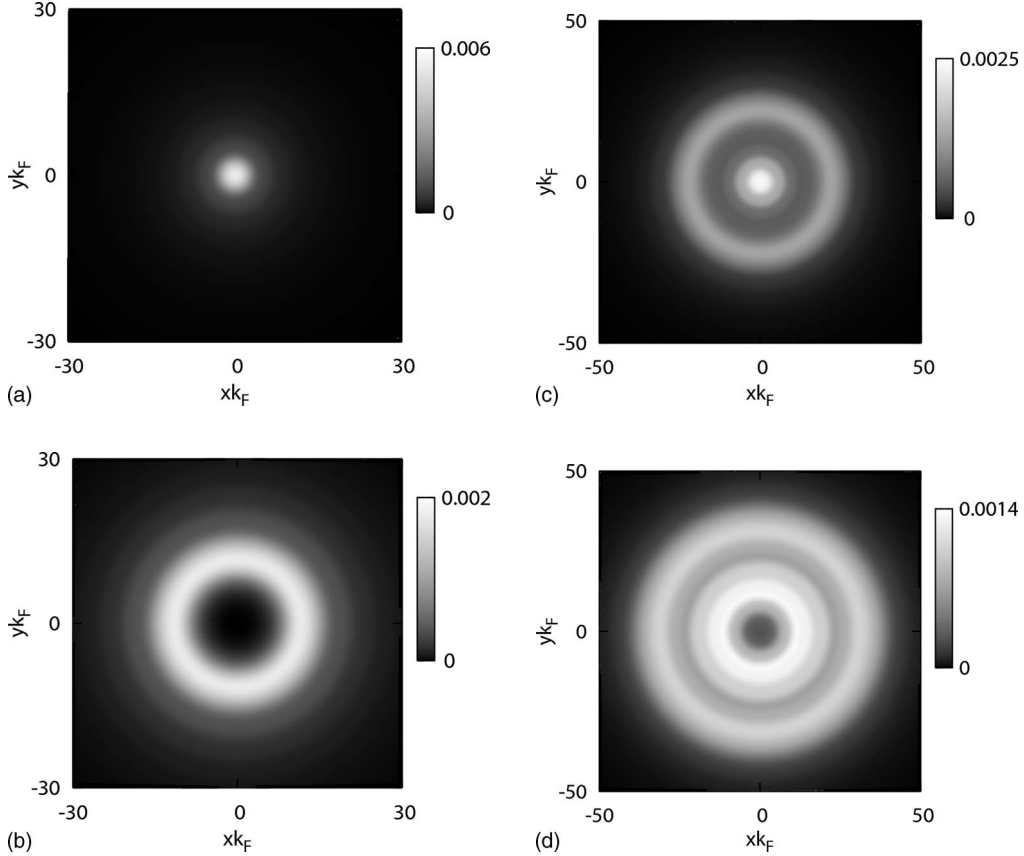FIG. 2. Local magnetization $m(x,y)$ around the vortex center in multiply quantized vortices with $w=1$ (a), 2 (b), 3 (c), and 4 (d). All the data are at $\delta\mu=0.02E_F$ and $T=0$, where $P=0.003$ (a), 0.002 (b), 0.005 (c), 0.005 (d).

the vortex center, e.g., for $w=2$, the CdGM branches in Fig. 1(b) become zero around $rk_F \simeq 12$, which is comparable with the coherence length $k_F\xi=20$. In addition, the number of the pseudozero energy state depends on the winding number of $\Delta(r)$. For instance, it is seen from Fig. 1(c) that the vortex state with $w=3$ has two pseudozero modes: The wave function of one mode has a peak at $r=0$ and the other is at $r \simeq 25k_F^{-1}$. Hence, it is numerically confirmed that the peak position and the number of the pseudozero energy states depends on the winding number w of vortices.

The presence of the splitting of the Fermi level between two spin states, i.e., $\delta\mu>0$, enables to reveal the two characteristic features of the CdGM states inside the giant vortex core, namely, (i) the pseudozero or gapful excitation at the core $r=0$ and (ii) the "pseudo" gapless excitation at $r \sim \xi$. Figure 2 shows the local "magnetization" profile

$$m(r) \equiv \rho_\uparrow(r) - \rho_\downarrow(r), \qquad (9)$$

around the core region of giant vortices with $w=1,2,3,4$. Here, $\rho_{\uparrow,\downarrow}(r)$ are the local particle densities in hyperfine spin states, which are given by

$$\rho_\uparrow(r) = \sum_q |u_q(r)|^2 f(E_q), \qquad (10a)$$

$$\rho_\downarrow(r) = \sum_q |v_q(r)|^2 [1-f(E_q)]. \qquad (10b)$$

The magnetization of the vortex core results from the fact that the excess atoms of the majority component can be accommodated by eigenstates with the pseudozero energy. For instance, the core of the single quantized ($w=1$) vortex is filled in by the paramagnetic moment, as seen in Fig. 2(a). The accommodation of the magnetic moment inside the core is associated with the low-lying quasiparticle state, i.e., the CdGM state. Since $\rho_{\uparrow,\downarrow}(r)=\int_{-\infty}^{\infty}\mathcal{N}_{\uparrow,\downarrow}(r,E)f(E)dE$ $\simeq \int_{-\infty}^{E_F^{(\uparrow,\downarrow)}}\mathcal{N}(r,E)dE$ at $T=0$, the local magnetization $m(r)$ is determined by the eigenstates embedded in the spacing between the Fermi surfaces of two spin species. Here, $\mathcal{N}(r,E)$ is the LDOS at $\delta\mu=0$, shown in Fig. 1. In the case of imbalanced population, the Fermi energy of the majority (minority) spin component is shifted from that of the balanced case upward (downward), $E_F^{(\uparrow)}=E_F+\delta\mu$ ($E_F^{(\downarrow)}=E_F-\delta\mu$). Hence, the low-lying CdGM states are embodied by the local paramagnetic moment inside the core, when $\delta\mu=0$.

For the odd-number vortex, since the lowest CdGM state at the vortex center has the much small energy $\sim\Delta_0^2/E_F$, the vortex center is always magnetized in the presence of the small splitting of the Fermi level $\delta\mu \ll \Delta_0$ as seen in Figs. 2(a) and 2(c). This is contrast to that in the even number vortex, where the vortex center cannot be magnetized in the situation of $\delta\mu \ll \Delta_0$ because of the large energy gap of the
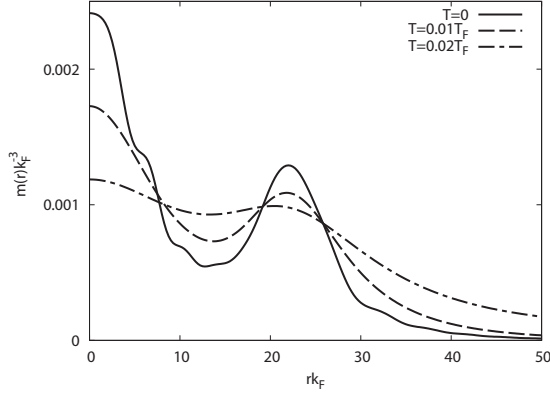
FIG. 3. Local magnetization around the core region of the w =3 vortex within $r < 50k_F^{-1}$ at $T/T_F = 0$ (solid), 0.01 (dashed), 0.02 (dashed-dotted line). The chemical potential shift is fixed as $\delta\mu$ =0.02E_F and max$|\Delta(r)|$=0.1E_F at T=0.

CdGM state. Furthermore, it is seen from Figs. 2(b)–2(d) that the pseudogapless excitation at $r \neq 0$ leads to the concentric oscillation pattern of the local magnetization, depending on the winding number w. For instance, in the case of the doubly quantized vortex with w=2 in Fig. 1(b), since the branches of the CdGM state touch the Fermi level at r =12k_F^{-1} and their excitations have almost zero energy, the excess atoms can be accommodated there under small splitting of the Fermi level $\delta\mu \ll \Delta_0$. The peak position of $m(\mathbf{r})$ at $r \sim 12k_F^{-1}$ in Fig. 2(b) coincides to the spatial profile of the pseudozero states in Fig. 1(b). The w=4 vortex has two crossing points of the CdGM branches on the Fermi level as seen in Fig. 1(d), leading to the double peak structure on the concentric circles with radius $rk_F \sim 15$ and 30 in Fig. 2(d).

We should mention the reason why the population imbalance P in Fig. 2 is extremely small. As we have mentioned above, the oscillation patterns in $m(\mathbf{r})$ are induced by the splitting of the Fermi level $\delta\mu$ smaller than the Pauli limit $\delta\mu_c = \Delta_0/\sqrt{2}$ [32]. In a system with a uniform pair potential, the superfluid pairing between the spin singlet fermions completely excludes the magnetization up to $\delta\mu < \delta\mu_c$, and the Pauli limit of the Fermi level splitting $\delta\mu = \delta\mu_c$ gives rise to a first order superfluid-normal phase transition with an abrupt jump of the local magnetization from the zero to finite value. In a system having a singular vortex, however, the imbalanced spin density can appear inside the vortex core as seen in Fig. 2, because the pair potential $\Delta(\mathbf{r})$ is strongly suppressed there. Hence, only the fermions inside the vortex core contribute to the net population imbalance P in Fig. 2. This is, however, peculiar to the uniform system without any background potential $V(\mathbf{r})$=0, and as shown later in Figs. 4 and 6, the presence of a harmonic potential can enhance the value of the population imbalance P, because the pair potential gradually weakens toward the outside of the trap.

Before turning to the unitary limit, we mention to the temperature dependence of the local magnetization inside the giant vortex core. Figure 3 shows the local magnetization around the core region $r \lesssim 50k_F^{-1}$ of the w=3 vortex at several temperatures $T/T_F = 0, 0.01, 0.02$, where $\delta\mu = 0.02E_F$ is fixed. It is found that the paramagnetic moment in the outside of the region $r > 30k_F^{-1}$ increases as T increases, which is char-

acterized by the Yosida function [33], while that at the vortex center (r=0) and at the concentric peak ($r \simeq 25k_F^{-1}$) decreases. The temperature comparable to $\delta\mu$ smooths the concentric peak structure in $m(r)$. In addition, it should be mentioned that since the oscillation patterns of the magnetization are produced by the occupation difference of the low-lying CdGM state having the energy close to the Fermi level, the experimental detection of the distinct pattern requires the temperature to be lower than the order of its level spacing $\sim \Delta_0^2/E_F$. For instance, $T < \Delta_0^2/E_F = 0.01E_F$ in the current situation with $\Delta_0 = 0.1E_F$.

III. GIANT VORTICES WITH POPULATION IMBALANCE: TRAPPED FERMI GASES NEAR FESHBACH RESONANCE

A. BCS-BEC crossover theory

Having obtained the direct relation between the quasiparticle structures and magnetization inside giant vortex cores in the weak-coupling limit, let us now proceed to extend the analysis into the more realistic situation, such as a trapped Fermi gas under an s-wave Feshbach resonance. Here, we consider the three-dimensional cylindrical system that the fermions are confined by the two-dimensional trap potential $V(\mathbf{r}) = \frac{1}{2}M\omega^2 r^2$, where $r^2 \equiv x^2 + y^2$. To do with the vicinity of s-wave Feshbach resonance, we have to modify the theoretical framework based on the BdG equation in Sec. II A. First, the ultraviolet divergence in Eq. (4) is removed by replacing g to the effective coupling constant $\tilde{g}$, which is associated with the energy cutoff E_c and the dimensionless coupling constant $1/(k_F a)$ [12,34],

$$\frac{E_F}{\tilde{g}k_F^3} = \frac{1}{8\pi k_F a} + \frac{1}{4\pi^2}\sqrt{\frac{E_c}{E_F}}, \quad (11)$$

where a is an s-wave scattering length. Also, the chemical potential μ is adjusted during the iteration to conserve the total particle number

$$N = N_\uparrow + N_\downarrow, \quad N_{\uparrow,\downarrow} = \int \rho_{\uparrow,\downarrow}(\mathbf{r})d\mathbf{r}, \quad (12)$$

where the particle density of each spin state is given by Eq. (10).

The BdG Eq. (2) is now self-consistently coupled with the particle number Eq. (12) and the regularized gap Eq. (4), where the bare coupling constant g in Eq. (4) is replaced to the effective one $\tilde{g}$ in Eq. (11). The set of equations is free from the energy cutoff E_c and allows one to describe the qualitative feature of T=0 superfluid phases in the entire range of $(k_F a)^{-1}$ from the BCS $[(k_F a)^{-1} \to -\infty]$ to the BEC limit $[(k_F a)^{-1} \to +\infty]$.

We numerically solve the gap Eq. (4) up to the energy $E^{(BdG)} = 100\omega_r$, by using the quasiparticle wave function obtained from Eq. (2). In addition, the higher energy contribution above $E^{(BdG)}$ is supplemented by employing the local density approximation (LDA). The details of the BdG-LDA hybrid method are described in Ref. [27]. For all data, the total particle number is conserved as N=9000, and we also

set $L=3d$, corresponding to the Fermi energy $E_F = \omega[30\pi Nd/(16L)]^{2/5} = 50\omega$. Here, the trap length and energy scales are introduced, i.e., $d \equiv \sqrt{1/M\omega}$ and ω, respectively. The calculation is carried out in the range from the weak-coupling regime $(k_F a)^{-1} = -1.2$ to the unitary limit $(k_F a)^{-1} = 0$.

B. Quasiparticle structure and local magnetization inside giant cores

Here, since in the actual experiment the net magnetization is conserved due to the absence of the spin relaxation process, it is convenient to introduce the population imbalance between two hyperfine spin states

$$P \equiv \frac{N_\uparrow - N_\downarrow}{N_\uparrow + N_\downarrow}. \tag{13}$$

Similarly to the nontrapped system in Fig. 2, it is found that the distinct pattern of the local "magnetization" $m(r)$ for vortices with arbitrary winding number appears inside the core in the weak-coupling regime $1/(k_F a) = -0.4, -1.2$, even in the presence of the trap potential. Note that the coherence length is estimated as $\xi \equiv k_F/(M\Delta_0) = 5.2k_F^{-1} = 0.52d$ at $1/(k_F a) = -0.4$ and $\xi = 16.7k_F^{-1} = 0.167d$ at $1/(k_F a) = -1.2$, where $\Delta_0 \equiv \max|\Delta(r)|$ at $T=0$. The magnetization profiles inside the $w=1,2,3$ vortex cores at $1/(k_F a) = -0.4$ are displayed in Figs. 4(a), 4(c), and 4(e), respectively, where the fermions are confined by the harmonic trap.

As the interaction approaches the unitary limit, however, the profile of $m(r)$ is drastically changed. Figures 4(b), 4(d), and 4(f) show the profile of the local magnetization around the giant vortex core at the unitary limit $1/k_F a = 0$, where the coherence length $\xi = 3.0k_F^{-1} = 0.3d$. In the vortex state with $w=1$ at $1/(k_F a) = 0$, the lowest CdGM state has a large energy gap comparable with Δ_0, because of $\Delta_0/E_F = O(1)$. Hence, the energy gap of the lowest CdGM state bounded on the vortex center leads to the absence of the magnetization inside the core even in the high value of P. Note that the large population imbalance in the $w=1$ vortex in Fig. 4(b) results from the magnetization accommodated around the edge region of the cloud, $r \gtrsim \xi$. This means that the volume of the magnetization $m(x,y)$ inside the core within $r/d < 1$ is almost the same in Figs. 4(a)–4(f).

At $1/(k_F a) = 0$, in the vortex state with $w>1$, we also find a completely different behavior of $m(r)$ from that at $1/(k_F a) = -0.4$. For instance, in contrast to the pattern shown in Figs. 2(b) and 4(c), the core of the doubly quantized vortex in Fig. 4(d) is filled in by a large number of excess fermions, which yields the single peak structure around the vortex center. Similarly, the small depletion of $m(r)$ appears at $r=0$ in the $w=3$ vortex on a resonance, which is contrast to that in Figs. 2(b) and 4(c).

The behavior of $m(r)$ in the core region of various giant vortices results from the strong-coupling effect with $\Delta_0/E_F \sim O(1)$ at $1/k_F a = 0$. To understand this, in Fig. 5(a), we first plot the energy shift of the peak of $\mathcal{N}(r=0,E)$ at $\delta\mu=0$, as functions of $1/(k_F a)$. As seen in Fig. 1(b), in the weak-coupling regime with $\Delta_0/E_F = 0.1$ and $\mu = E_F$, the LDOS's $\mathcal{N}_{\uparrow,\downarrow}(r=0,E)$ of the $w=2$ vortex yield the double peak struc-

tures at $E \simeq \pm 0.7\Delta_0$ on the vortex center, whose spectral evolution is almost symmetric with respect to the Fermi level $E=0$. At $1/k_F a = 0$, however, the double peaks of $\mathcal{N}_{\uparrow,\downarrow}(r=0,E)$ in the $w=2$ vortex are shifted upward and their positions become asymmetric with respect to the Fermi energy, as seen in Fig. 5(a) with the solid line. Here the lower branch stays near the $E \sim 0$ region in the $1/(k_F a) \sim 0$ region. This shift is understandable from the analytic expression of the CdGM state shown in Eq. (7),

$$E_q^{(w=2)} = \omega_0 \pm \frac{1}{2}\omega_1, \tag{14}$$

with $q_\theta = 0$, $q_z = 0$, and $n=0,-1$. Here, let us recall that ω_0 and ω_1 are of the order of $\frac{\Delta_0^2}{E_F}$ and Δ_0, respectively, i.e., $\omega_0 \ll \omega_1$ in the weak-coupling regime. Then, the eigenenergies of two lowest CdGM states in the $w=2$ vortex are symmetric with respect to the Fermi level $E=0$. Indeed, as plotted at $1/(k_F a) = -1.2$ in Fig. 5(a), the point below (above) $E=0$ corresponds to the plus (minus) sign of Eq. (14). Approaching the unitary limit $1/k_F a = 0$, however, ω_0 becomes comparable to ω_1, which causes the energy shift of the CdGM state with $\omega_0 - \frac{1}{2}\omega_1$ located inside the Fermi level toward $E=0$, e.g., $E = -0.05\Delta_0$ at $1/(k_F a) = 0$ in Fig. 5(a). These energy shifts of the CdGM states localized on the center of giant vortices are also confirmed in Ref. [19], where the CdGM states shift up across $E=0$ approaching the BEC limit $[1/(k_F a) \rightarrow +\infty]$.

Figure 5(b) shows the LDOS at $r=0$ in $w=2$ vortex state with and without population imbalance at $1/k_F a = 0$. In a finite population imbalance, since the energy of two spin states is shifted downward ($\uparrow$ spins) or upward ($\downarrow$ spins), the lower branch of the two CdGM states is occupied (unoccupied) by the majority (minority) spin component, which gives rise to the magnetization of the vortex center even in the even number winding vortex.

Figure 5(a) also tells us that as $1/(k_F a)$ approaches unitarity, the pseudozero eigenstate, which appears in the $w=3$ vortex at $1/(k_F a) = -1.2$, is quickly shifted upward, e.g., $E = 20\omega = 0.57\Delta_0$ at unitarity, as seen in Figs. 5(a) and 5(c). It indicates that at $1/k_F a = 0$, the distinct energy gap may emerge in the vicinity of $E=0$ in the case of the odd number w. This energy gap leads to the suppression of $m(r)$ at $r=0$ as seen in Fig. 4(f). This is in contrast to the case of the weak-coupling regime. For instance, as seen in Fig. 4(e), the magnetization in the $w=3$ vortex at $1/(k_F a) = -0.4$ has a distinct peak at $r=0$ and also another peak on the concentric circles. This oscillation pattern of $m(r)$ becomes clear approaching the weak-coupling limit $[1/(k_F a) \rightarrow -\infty]$.

In addition, we mention that due to the presence of the trap potential, finite population imbalance and depairing occurs in the vicinity of the edge, in addition to the inner region of the core. The numerical results for the pairing field and local magnetization shown in Fig. 6 reveals the phase separated state between the superfluid and spin polarized normal domains at $1/k_F a = 0$. Similarly to the nonvortex [27] and the case of singly quantized vortex [26], the pairing field in $1/k_F a < 0$ yields an oscillation in the surface region, that is,
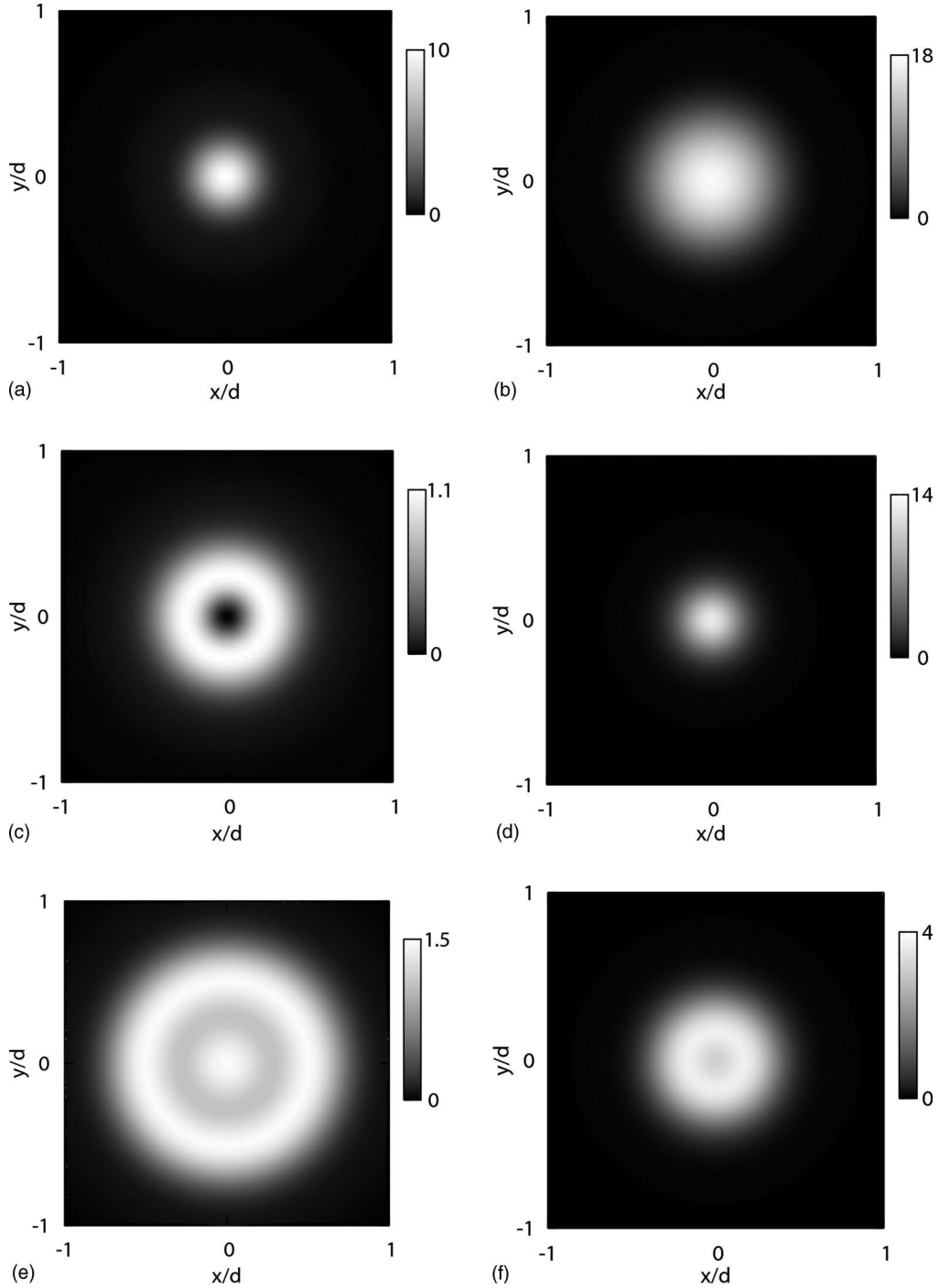
FIG. 4. Local magnetization $m(x,y)$ around the vortex core with the winding number $w=1$ (a),(b); 2 (c),(d); 3 (e),(f) at $T=0$. (a), (c), and (e) are in the BCS side of the resonance $1/(k_F a)=-0.4$, and the others are at the resonance $1/(k_F a)=0$. Population imbalance is estimated as (a) $P=0.12$ ($w=1$), (b) 0.82 ($w=1$), (c) 0.014 ($w=2$), (d) 0.03 ($w=2$), (e) 0.014 ($w=3$), (f) 0.03 ($w=3$).

the Fulde-Ferrell-Larkin-Ovchinnikov-like oscillation. It is found that the oscillation of $\Delta(r)$ is proper to imbalanced systems both with and without a vortex line in the extensive range $1/k_F a < 0$. As the interaction touches the unitary limit, however, the coexistence area becomes narrow, since the oscillation period is reduced to the interparticle distance $\sim k_F^{-1}$ [27].

IV. CONCLUDING REMARKS

In this paper, we have investigated the core structure of multiply quantized vortex in imbalanced Fermi systems with and without a trap potential. In conclusion, it is found that in the weak-coupling regime, as shown in Fig. 2, the local magnetization inside the core of multiply quantized vortices yields the concentric oscillation pattern, which reveals the
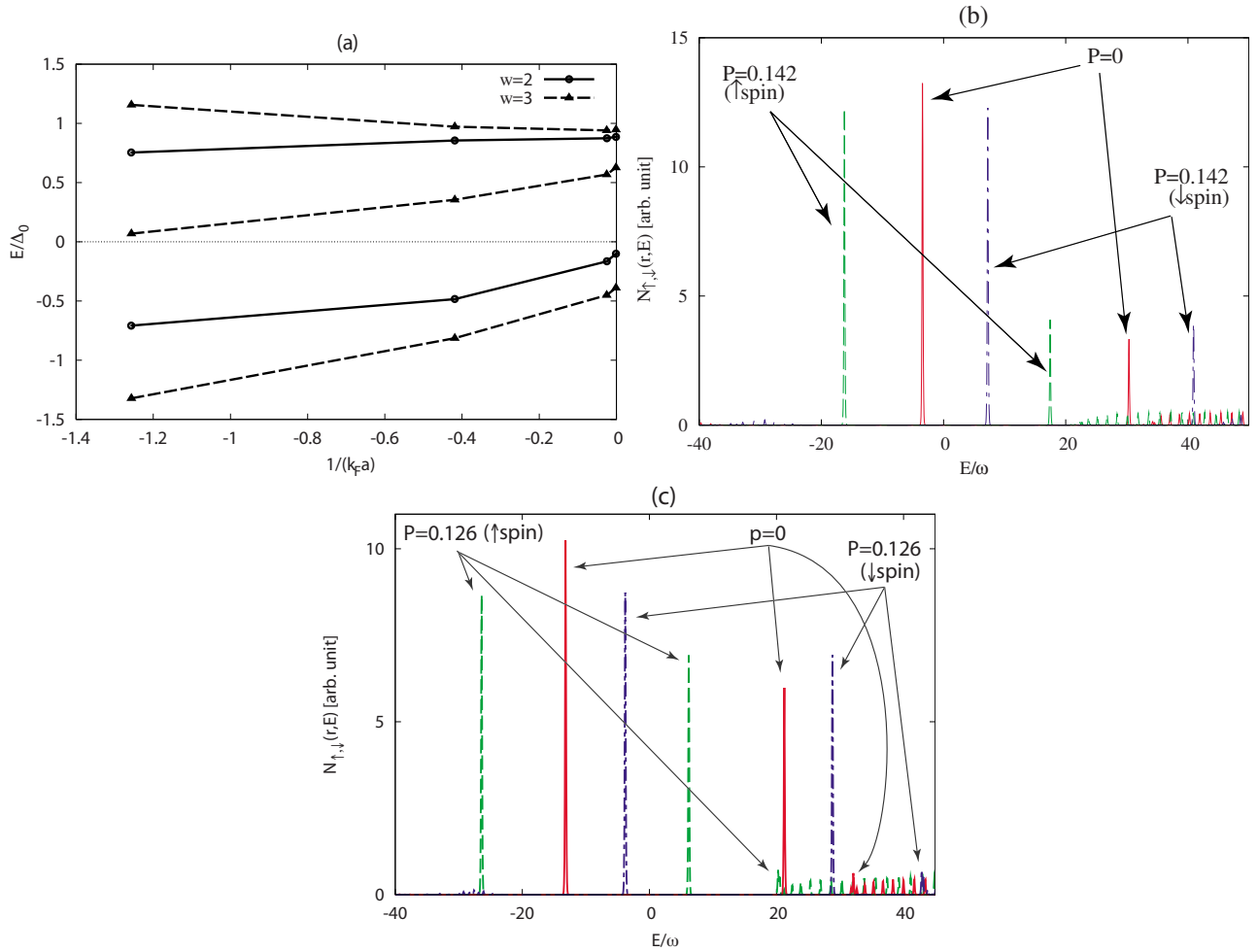
FIG. 5. (Color online) (a) Eigenenergies of the CdGM states having the intensity at $r=0$ as functions of $1/(k_F a)$. The solid and dashed lines denote the CdGM branch in the $w=2$ and 3 vortex states, respectively. The eigenenergies in (a) are scaled by Δ_0, which is given by $\Delta_0 \equiv \max|\Delta(\boldsymbol{r})|$. LDOS at $r=0$, $N_{\uparrow,\downarrow}(r,E)$, of $w=2$ (b) and 3 (c) vortex state with and without population imbalance. The all dates in (b) and (c) are at $1/k_F a=0$.

quasiparticle structure bound inside the core, called the CdGM states. The "pseudozero" energy of the CdGM states in vortices with an odd-winding number enables the accommodation of the magnetization on the vortex center. In contrast, the magnetic moment is excluded from the vortex center in the case of an even winding number. This is because the CdGM state has a distinct energy gap of the order of Δ_0 as shown analytically in Eq. (7) and numerically in Fig. 1. Note that the clear oscillation patterns in the weak-coupling regime require the temperature to be lower than the order of the level spacing of the CdGM states $\sim \Delta_0^2/E_F$.

This difference of the magnetization profile is alternatively understandable from the π-phase shift of the pairing field [29,35–38]. In general, in the presence of the kink structure of the pair potential, quasiparticles across the domain wall feel the sign change of the pair potential, giving rise to the eigenmodes with the zero energy, called the Andreev bound state [39] or the midgap state [35–37]. The modes are strongly bounded around the domain wall. In the case of giant vortices with an odd winding number, since quasiparticles tracing the path across the vortex center $r=0$ always experience the π-phase shift of $\Delta(\boldsymbol{r})$, the bound state, called

the CdGM state with the pseudozero energy in the text, appears in the vicinity of the Fermi level, whose energy scale is much smaller than the energy gap in the bulk region. In contrast, the pseudozero modes never appear in case of an even winding number, where the pair potential does not change its sign along the path across the vortex center. The relation between the topological structure of $\Delta(\boldsymbol{r})$ and the quasiparticle state has been shown analytically in Eq. (7) and numerically in Fig. 1. The pseudozero CdGM states can easily participate the magnetization, when the Fermi level of two spin states is mismatched. The peak structure of the local magnetization appears at $r=0$ in Figs. 2(a) and 2(c). In the even number of winding, however, the distinct energy gap arising from the topological reason prevents the accommodation of the excess spins at $r=0$, as seen in Figs. 2(b) and 2(d).

In contrast to the weak-coupling regime, where the magnetization inside vortex cores can be closely associated with the topological structure of the pairing field, it has been found that the magnetization profile inside the core of various giant vortices is drastically changed in the vicinity of Feshbach resonance. The key factor is that two energy scales
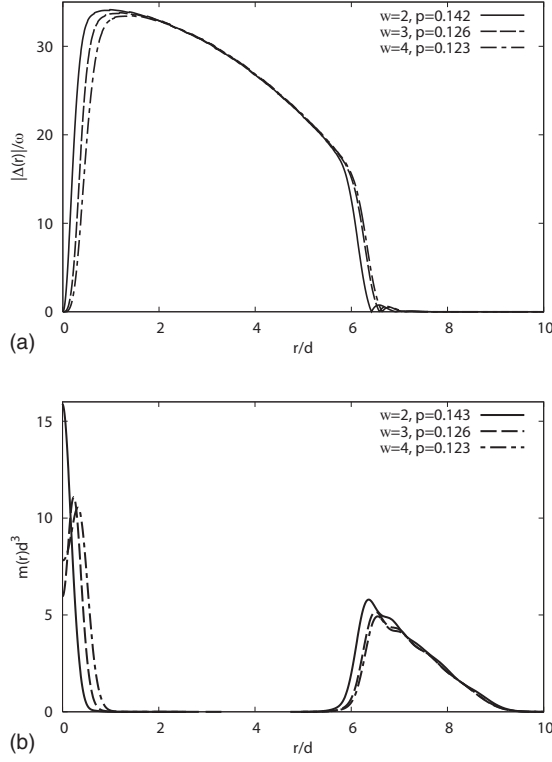
FIG. 6. Profile of the local pair potential $\Delta(r)$ (a) and magnetization $m(r)$ (b) at the unitary limit $1/k_F a = 0$. Population imbalance is estimated in vortex states with various winding number as $P = 0.143$ ($w=2$, solid line), 0.126 ($w=3$, dashed line), 0.123 ($w=4$, dashed-dotted line).

in Eq. (7), ω_0 and ω_1, become comparable as $1/k_F a$ approaches the unitary limit. The upward shift of all core bound states gives rise to a larger change of the magnetization profile inside the cores from that in the BCS limit.

Finally, we should emphasize that the oscillating pattern of the magnetization inside the giant core provides the spectroscopy of the discretized core structures. As seen in Fig. 4, the magnetization profile inside the core is drastically changed as $1/(k_F a)$ varies. Namely, it is proposed that the density experiments using phase contrast imaging reveal the spectrum of the core localized CdGM states via the magnetization.

ACKNOWLEDGMENTS

APPENDIX: ANALYTIC SOLUTION OF CdGM STATES IN GIANT VORTICES

In this appendix, we describe the details on the derivation of the analytic expression of CdGM states in Eq. (7), from the BdG Eq. (2) without the chemical potential shift $\delta\mu = 0$ and trap potential $V(r) = 0$. Using Eqs. (1) and (3) and assuming $q_z \equiv k_\mu \sqrt{1 - \sin^2(\alpha)} \ll k_\mu \equiv \sqrt{2M|\mu|^2}$, the BdG Eq. (2) can be rewritten in the cylindrical coordinate to

$$
[\mathcal{L}_m \hat{\tau}_0 - 2iM\Delta\hat{\tau}_2]\boldsymbol{u_q} = \hat{\tau}_3 \left[\frac{w\left(q_\theta - \dfrac{w}{2}\right)}{r^2} - 2ME_q \right]\boldsymbol{u_q}.
$$

(A1)

Here we set $\Delta \equiv \Delta(r)$, $\boldsymbol{u_q} \equiv \boldsymbol{u_q}(r) = [u_q(r), v_q(r)]^T$, and

$$
\mathcal{L}_m \equiv \frac{d^2}{dr^2} + \frac{1}{r}\frac{d}{dr} - \frac{m^2}{r^2} + k_\mu^2 \sin^2(\alpha)
$$

(A2)

with $m = \sqrt{q_\theta^2 - wq_\theta + \frac{w^2}{2}}$. Also, we use the Pauli matrices $\hat{\tau}_{1,2,3}$ and 2×2 unit matrix $\hat{\tau}_0 = \text{diag}(1,1)$. Throughout this appendix, we consider the BCS regime with $\mu > 0$.

Following the procedure proposed by Caroli *et al.* [3], we introduce a radius r_c that $\Delta(r) = 0$ for $r < r_c$. Then, the BdG Eq. (A1) can be analytically solved if one assumes the following conditions: (i) $|q_\theta| \ll r_c k_F \ll k_F \xi$, (ii) $E_q \ll \Delta_0$, and (iii) $E_q \ll |\mu|^2 \sin^2(\alpha)$.

The wave function in Eq. (A1) is obtained in the range $r < r_c$ as

$$
\boldsymbol{u_q}(r) = \begin{bmatrix} A_u J_{q_\theta}(k_+(\alpha)r) \\ A_v J_{q_\theta - w}(k_-(\alpha)r) \end{bmatrix},
$$

(A3)

where A_u and A_v are the arbitrary constant and we set

$$
k_\pm(\alpha) \equiv k_\mu \sin(\alpha) \pm \frac{E_q}{v_\mu(\alpha)},
$$

(A4)

with $v_\mu(\alpha) = k_\mu \sin(\alpha)/M$. For $r > r_c$, the wave functions are composed of the Hankel function $H_m^{(i)}$ and the slow functions $\boldsymbol{\varphi}_i(r)$ varying over the order of ξ [3],

$$
\boldsymbol{u_q}(r) = \sum_{i=1,2} H_m^{(i)}(k_\mu \sin(\alpha)r)\boldsymbol{\varphi}_i(r).
$$

(A5)

Then, Eq. (A1) can be reduced to

$$
\left[\hat{\tau}_0 \frac{d}{dr} - \hat{\tau}_2 \frac{\Delta}{v_\mu} \right]\boldsymbol{\varphi}_1 = i\hat{\tau}_3 \left[\frac{E_q}{v_\mu} - \frac{w\left(q_\theta - \dfrac{w}{2}\right)}{2Mv_\mu r^2} \right]\boldsymbol{\varphi}_1
$$

(A6)

and $\boldsymbol{\varphi}_2(r) \propto \boldsymbol{\varphi}_1^*(r)$. Here, we set $v_\mu \equiv v_\mu(\alpha)$ and $\boldsymbol{\varphi}_1 \equiv \boldsymbol{\varphi}_1(r)$. Under the conditions (i)–(iii) described above, the right-hand side of Eq. (A6) can be regarded as the small perturbation. We now assume the solution of Eq. (A6) as

$$
\boldsymbol{\varphi}_1(r) = \boldsymbol{\varphi}_1^{(0)}(r) + iB_1 e^{-\chi(r)} \begin{bmatrix} \psi_1(r) \\ -i\psi_2(r) \end{bmatrix},
$$

(A7)

where $\boldsymbol{\varphi}_1^{(0)}(r)$ is the solution when the right-hand side of Eq. (A6) is neglected, and $\psi_{1,2}(r)$ is the small correction to $\boldsymbol{\varphi}_1^{(0)}(r)$, i.e., $|\psi_{1,2}(r)| \ll 1$. Hence, one finds $\varphi_1^{(0)}(r) = B_1 e^{-\chi(r)}[1, -i]^T$ with

$$
\chi(r) \equiv \frac{1}{v_\mu(\alpha)} \int_0^r \Delta(r')dr'.
$$

(A8)

Since $|\psi_{1,2}(r)| \ll 1$, Eq. (A7) can be also expressed as

$$\boldsymbol{\varphi}_1(r) \simeq B_1 e^{-\chi(r)} \begin{bmatrix} e^{i\psi_1(r)} \\ -ie^{i\psi_2(r)} \end{bmatrix}. \qquad \text{(A9)}$$

Within Eq. (A7), one can find the solution of Eq. (A6) as

$$\psi_1(r) = -\psi_2(r) \equiv \psi(r) = -\int_r^\infty \left(\frac{E_q}{v_\mu} - \frac{w\left(q_\theta - \frac{w}{2}\right)}{2Mv_\mu r'^2} \right)$$
$$\times e^{-2\{[\chi(r')-\chi(r)]\}} dr', \qquad \text{(A10)}$$

where we set $v_\mu \equiv v_\mu(\alpha)$, again.

To get the solution of the BdG Eq. (A1), the wave functions in two different domains, Eq. (A3) for $r < r_c$ and (A5) for $r > r_c$, are now matched at $r \sim r_c$. Because of the condition (i), $|q_\theta| \ll r_c k_F$, making use of the asymptotic forms of $J_\nu(z)$ and $H_\nu^{(1,2)}(z)$ in $z \gg |\nu|$, the wave functions for $r < r_c$ in Eq. (A3) are rewritten as

$$u_q \simeq \sqrt{\frac{2M}{\pi v_\mu r}} A_u \cos\left(k_+ r + \frac{q_\theta^2 - \frac{1}{4}}{2k_+ r} - \frac{2q_\theta + 1}{4}\pi \right), \qquad \text{(A11a)}$$

$$v_q \simeq \sqrt{\frac{2M}{\pi v_\mu r}} A_v \cos\left[k_- r + \frac{(q_\theta - w)^2 - \frac{1}{4}}{2k_- r} - \frac{2q_\theta - 2w + 1}{4}\pi \right] \qquad \text{(A11b)}$$

with $v_\mu \equiv v_\mu(\alpha)$ and $k_\pm \equiv k_\pm(\alpha)$. Also, Eq. (A5) with Eq. (A9) for $r > r_c \gg |q_\theta|/k_F$ is

$$\boldsymbol{u}_q \simeq \sqrt{\frac{2M}{\pi v_\mu r}} e^{-\chi(r)} \begin{bmatrix} B_1 e^{i\eta_+(r)} + B_2 e^{-i\eta_+(r)} \\ -iB_1 e^{i\eta_-(r)} + iB_2 e^{-i\eta_-(r)} \end{bmatrix} \qquad \text{(A12)}$$

with

$$\eta_\pm(r) \equiv Mv_\mu r + \frac{m^2 - \frac{1}{4}}{2Mv_\mu r} - \frac{2m+1}{4}\pi \pm \psi(r). \qquad \text{(A13)}$$

To match two expressions of $u_q(r)$ in Eqs. (A11a) and (A12) at $r = r_c$, one should put the coefficients $B_{1,2}$ as

$$B_1 = \frac{A_u}{2} e^{i\gamma}, \quad B_2 = \frac{A_u}{2} e^{-i\gamma}. \qquad \text{(A14)}$$

By comparing with Eqs. (A11a) and (A12), one can obtain the expression of ψ as

$$\psi(r) \simeq \frac{E_q}{v_\mu} r + \frac{w\left(q_\theta - \frac{w}{2}\right)}{2Mv_\mu r} + \frac{m - q_\theta}{2}\pi - \gamma. \qquad \text{(A15)}$$

In a same way, one finds the another expression from Eqs. (A11b) and (A12)

$$\psi(r) \simeq \frac{E_q}{v_\mu} r + \frac{w\left(q_\theta - \frac{w}{2}\right)}{2Mv_\mu r} - \frac{m - q_\theta + w}{2} + \gamma - \left(n + \frac{1}{2}\right)\pi, \qquad \text{(A16)}$$

where n is the integer. The expressions on $\psi(r)$ in Eqs. (A15) and (A16) become identical when γ satisfies

$$\gamma = \frac{\pi}{2}\left(m - q_\theta + \frac{w+1}{2} \right) + \frac{\pi}{2} n. \qquad \text{(A17)}$$

The alternative expressions of $\psi(r)$ in Eqs. (A10) and (A15) with Eq. (A17) should be identical at $r = r_c$. Hence, we finally obtain the eigenvalue of the BdG Eq. (2),

$$E_q = -\left(q_\theta - \frac{w}{2} \right) \frac{\omega_0}{\sin(\alpha)} + \left(n + \frac{w-1}{2} \right)\sin(\alpha)\omega_1, \qquad \text{(A18)}$$

where

$$\omega_0 \equiv \frac{w \int_{r_c}^\infty \frac{\Delta(r')}{k_\mu r'} e^{-2\chi(r')} dr'}{\int_0^\infty e^{-2\chi(r')} dr'}, \qquad \text{(A19a)}$$

$$\omega_1 \equiv \frac{\pi k_\mu}{2M \int_0^\infty e^{-2\chi(r')} dr'}. \qquad \text{(A19b)}$$

To estimate the order of the energy scale of $\omega_{0,1}$, let us consider the simplest case of $\Delta(r)$, that is, $\Delta(r) = \Delta_0 \tanh(r/\xi)$. In this situation, one find $\omega_1 \simeq \frac{\pi}{2}\Delta_0$ and $\omega_0 = g\frac{w}{2}\frac{\Delta_0^2}{E_F}$ with $\int_0^\infty e^{-2\chi(r')} dr' = \xi$. Here, $g \sim O(1)$. Hence, the eigenvalue E_q is composed of two different energy scales, such as Δ_0 and Δ_0^2/E_F. The expression in the case of a singly quantized vortex ($w=1$) coincides to that in Ref. [3], and that with an arbitrary w reproduces the results within the semiclassical approximation in Ref. [18]. The further details on Eq. (A18) is described in Sec. II B. We should mention that the integrals in ω_0 and ω_1 depends on the winding number of $\Delta(r)$.

[1] A. L. Fetter and A. A. Svidzinsky, J. Phys.: Condens. Matter **13**, R135 (2001).

[2] K. Kasamatsu and M. Tsubota, e-print arXiv:0709.1042.

[3] C. Caroli, P. G. De Gennes, and J. Matricon, Phys. Lett. **9**, 307 (1964).

[4] N. Hayashi, T. Isoshima, M. Ichioka, and K. Machida, Phys. Rev. Lett. **80**, 2921 (1998).

[5] N. Hayashi, M. Ichioka, and K. Machida, J. Phys. Soc. Jpn. **67**, 3368 (1998).

[6] N. Nygaard, G. M. Bruun, C. W. Clark, and D. L. Feder, Phys.

Rev. Lett. **90**, 210402 (2003).

[7] N. Nygaard, G. M. Bruun, B. I. Schneider, C. W. Clark, and D. L. Feder, Phys. Rev. A **69**, 053622 (2004).

[8] A. Bulgac and Y. Yu, Phys. Rev. Lett. **91**, 190404 (2003).

[9] M. Machida and T. Koyama, Phys. Rev. Lett. **94**, 140401 (2005).

[10] M. Machida, Y. Ohashi, and T. Koyama, Phys. Rev. A **74**, 023621 (2006).

[11] C.-C. Chien, Y. He, Q. Chen, and K. Levin, Phys. Rev. A **73**, 041603(R) (2006).

[12] R. Sensarma, M. Randeria, and T.-L. Ho, Phys. Rev. Lett. **96**, 090403 (2006).

[13] M. W. Zwierlein, J. R. Abo-Shaeer, A. Schirotzek, C. H. Schunck, and W. Ketterle, Nature (London) **435**, 1047 (2005).

[14] G. E. Volovik, JETP Lett. **57**, 244 (1993).

[15] Y. Tanaka, A. Hasegawa, and H. Takayanagi, Solid State Commun. **85**, 321 (1993).

[16] S. M. M. Virtanen and M. M. Salomaa, Phys. Rev. B **60**, 14581 (1999).

[17] K. Tanaka, I. Robel, and B. Jankó, Proc. Natl. Acad. Sci. U.S.A. **99**, 5233 (2002).

[18] K. P. Duncan and B. L. Györffy, Physica C **404**, 153 (2004).

[19] H. Hu and X.-J. Liu, Phys. Rev. A **75**, 011603(R) (2007).

[20] A. E. Leanhardt, A. Görlitz, A. P. Chikkatur, D. Kielpinski, Y. Shin, D. E. Pritchard, and W. Ketterle, Phys. Rev. Lett. **89**, 190403 (2002).

[21] Y. Shin, M. Saba, M. Vengalattore, T. A. Pasquini, C. Sanner, A. E. Leanhardt, M. Prentiss, D. E. Pritchard, and W. Ketterle, Phys. Rev. Lett. **93**, 160406 (2004).

[22] M. Kumakura, T. Hirotani, M. Okano, Y. Takahashi, and T. Yabuzaki, Phys. Rev. A **73**, 063605 (2006).

[23] V. Bretin, S. Stock, Y. Seurin, and J. Dalibard, Phys. Rev. Lett. **92**, 050403 (2004).

[24] C. Ryu, M. F. Andersen, P. Cladé, K. Vasant Natarajan Helmerson, and W. D. Phillips, Phys. Rev. Lett. **99**, 260401 (2007).

[25] H. Hu, X.-J. Liu, and P. D. Drummond, Phys. Rev. Lett. **98**, 060406 (2007).

[26] M. Takahashi, T. Mizushima, M. Ichioka, and K. Machida, Phys. Rev. Lett. **97**, 180407 (2006).

[27] T. Mizushima, M. Ichioka, and K. Machida, J. Phys. Soc. Jpn. **76**, 104006 (2007).

[28] T. Mizushima, K. Machida, and M. Ichioka, Phys. Rev. Lett. **94**, 060404 (2005).

[29] T. Mizushima, K. Machida, and M. Ichioka, Phys. Rev. Lett. **95**, 117003 (2005).

[30] K. Machida, T. Mizushima, and M. Ichioka, Phys. Rev. Lett. **97**, 120407 (2006).

[31] F. Gygi and M. Schlüter, Phys. Rev. B **43**, 7609 (1991).

[32] A. M. Clogston, Phys. Rev. Lett. **9**, 266 (1962).

[33] K. Yosida, Phys. Rev. **110**, 769 (1958).

[34] C. A. R. Sá de Melo, M. Randeria, and J. R. Engelbrecht, Phys. Rev. Lett. **71**, 3202 (1993).

[35] K. Machida and H. Nakanishi, Phys. Rev. B **30**, 122 (1984).

[36] K. Machida and M. Nakano, Phys. Rev. Lett. **55**, 1927 (1985).

[37] K. Machida and M. Nakano, Phys. Rev. B **34**, 5073 (1986).

[38] M. Ichioka, H. Adachi, T. Mizushima, and K. Machida, Phys. Rev. B **76**, 014503 (2007).

[39] S. Kashiwaya and Y. Tanaka, Rep. Prog. Phys. **63**, 1641 (2000).